

Two Photon Correlation in Anisotropic Quark-gluon plasma (aQGP).

Payal Mohanty, Mahatsab Mandal and Pradip K Roy*

HENPP Division, Saha Institute of Nuclear Physics, 1/AF, Bidhannagar, Kolkata 700064, India

(Dated: September 24, 2018)

The only way to obtain the space-time structure of heavy ion collision is through the study of two-particle momentum correlations. Thus we have studied the intensity correlation for the photons at most central collision at RHIC energy having fixed transverse momentum of one of the photons ($k_{1T} = 2$ GeV) to have an idea about the emission zone in presence of initial momentum space anisotropy. For the evolution in aQGP, the *free streaming interpolating* model with fixed initial condition has been used. Whereas for the space-time evolution for both the isotropic Quark Gluon Plasma (iQGP) and the hadronic phases, relativistic (1+2)d hydrodynamics model with cylindrical symmetry and boost invariance along longitudinal direction has been used. The variation of Bose-Einstein correlation function (BECF), C_2 , for two identical photons as a function of q_{out} , q_{side} and q_{long} is evaluated. Our analysis is based on the sensitivity of the momentum space anisotropy on the correlation function and also on the extracted HBT radii from it. It is observed that the value of C_2 as function of q 's is reduced for anisotropic scenario compared to that of isotropic case for all the directions. As a result, the spatial dimension of the reaction zone increases due to the presence of momentum space anisotropy in the medium in all directions.

PACS numbers: 25.75.+r, 25.75.-q, 12.38.Mh

I. INTRODUCTION

The prime objective of heavy ion collisions (HIC) at relativistic energies is to create and explore the properties of novel state of partonic matter, known as Quark Gluon Plasma (QGP). Recently, enormous experimental efforts at Relativistic Heavy Ion Collider (RHIC) and Large Hadron Collider (LHC) are carried out in this direction. The method of two particle intensity interferometry, commonly known as Hanbury-Brown and Twiss (HBT) interferometry [1], has been used extensively in both theory and experiment to obtain the spatial and temporal informations of the particle emission zones created in HIC [2–4]. This method was first introduced in HIC in the hadronic sector through the study of quantum statistical correlation between identical pions which provided valuable inputs for the space-time description of the system at the freeze out surface [3]. In contrast to hadrons, the study of two-particle intensity interferometry of electromagnetic (EM) radiations, such as photon and dilepton interferometry [5–11], are more effective as they shed light on the dynamics of the collision from the entire evolution. Owing to large mean free path compared to the size of the system formed in HIC, the EM radiations travel unscathed from the entire evolution of the fireball without further re-scattering with the surrounding medium and hence can provide information of the history of evolution of the hot matter created in HIC [12–16].

The hydrodynamical model proposed by Bjorken [17] takes care of the evolution dynamics and is used with great triumph to describe the heavy ion collision data which assumes the system to be in local thermal equilibrium and isotropy in momentum space. However, the thermalization in the HIC is a debatable issue. Due to poor knowledge of the isotropization and thermalization time scales (τ_{iso} and τ_{therm} respectively), one need not assume the hydrodynamical behavior from the very beginning. There is an additional factor that needs to be highlighted here. In a realistic scenario, due to the rapid longitudinal expansion at the onset of the QGP phase, anisotropy arises in $p_T - p_L$ plane with $\langle p_L^2 \rangle \ll \langle p_T^2 \rangle$ in the local rest frame. With time, such asymmetry dies out with secondary partonic interactions. After which the system is considered to be isotropic and thermalized at proper time τ_{iso} and beyond $\tau \geq \tau_{iso}$ the system can be treated hydrodynamically. To include such momentum anisotropy in pre-equilibrium stage of the QGP phase, a simple phenomenological model is adopted from refs. [18–20]. In accordance with this model, there are two parameters: plasma momentum space anisotropy (ξ) and the hard momentum scale (p_{hard}) which take care of the anisotropic effect. We assumed two time scales here; (i) the initial QGP formation time, τ_i , and (ii) the isotropization time, τ_{iso} , when the isotropy in momentum space is achieved and they should fulfill the criteria that $\tau_i \leq \tau_{iso}$. In absence of anisotropy, $\tau_i = \tau_{iso}$.

In the present work, we study photon interferometry at most central RHIC initial conditions at $\sqrt{s_{NN}} = 200$ GeV including momentum anisotropy in the pre-equilibrium QGP phase. We devote our analysis for full evolution of the fireball to observe the

*Electronic address: Payal.Mohanty@saha.ac.in, mahatsab.mandal@saha.ac.in, pradip.roy@saha.ac.in

anisotropic effect on the size of the emission zone. Such an analysis helps in understanding the effect of anisotropy on the space-time dynamics of the evolving source. The free streaming interpolating model with fixed initial condition has been used for evolution in aQGP and (1+2)d hydrodynamical model with cylindrical symmetry and longitudinal boost invariance is used for $\tau \geq \tau_{iso}$. Here we have relaxed the assumption of local isotropy and considered the plasma with local anisotropy in $p_T - p_L$ plane in pre-equilibrium aQGP phase. We have assumed the following two sets of initial conditions for the analysis; SET-I: $\tau_i=0.147$ fm/c, $T_i= 446$ MeV and SET-II: $\tau_i=0.24$ fm/c, $T_i= 350$ MeV. In the present approach, we adopt two-stage evolution scenario. For aQGP evolution we use τ_i and T_i as the initial conditions. However, for hydrodynamic evolution, i.e. iQGP evolution τ_{iso} and $p_{hard}(\tau_{iso})$ can be considered as the initial conditions. The thermalized isotropic QGP is assumed with sufficiently high energy densities at $\tau = \tau_{iso}$. Afterwards, with expansion, the energy density reduces, hadronization begins at τ_q (pure QGP phase ends here). The system then undergoes a phase transition at transition temperature (T_c) and transforms to a hadronic gas phase at τ_h . With further expansion, the energy density reduces further and finally reaches freeze-out at T_f , called freeze-out temperature at freeze-out time (τ_f). In this work, we shall study the sensitivity of the two-photon correlation functions on the isotropization time (τ_{iso}), whereas the authors in [10] have investigated the behaviour of correlation functions by varying the formation time (τ_i).

The article is organized as follows. We have started with the definition and formulation of Bose-Einstein correlation function (BECF) in Sec. II. The thermal emission rate of photons used for the present calculation is discussed in Sec. III. The model used for space - time evolution is briefly outlined in Sec. IV. In Sec. V we discuss the sensitivity of our results to the initial momentum anisotropy with varying τ_{iso} . Finally we summarize in Sec. VI.

II. DEFINITION AND FORMALISM

The Bose-Einstein correlation function (BECF) for two photons with momenta \vec{k}_1 and \vec{k}_2 is defined as,

$$C_2(\vec{k}_1, \vec{k}_2) = \frac{P_2(\vec{k}_1, \vec{k}_2)}{P_1(\vec{k}_1)P_1(\vec{k}_2)} \quad (1)$$

where

$$P_1(\vec{k}) = \int d^4x \omega(x, k); \quad \omega(x, k) = E \frac{dR}{d^3k} \quad (2)$$

and

$$P_2(\vec{k}_1, \vec{k}_2) = P_1(\vec{k}_1)P_1(\vec{k}_2) + \frac{1}{2} \int d^4x_1 d^4x_2 \omega(x_1, K)\omega(x_2, K) \cos(\Delta x^\mu \Delta k_\mu) \quad (3)$$

where $\vec{k}_i = (k_{iT} \cos \psi_i, k_{iT} \sin \psi_i, k_{iT} \sinh y_i)$ is the three momentum of the two identical photons with $i = 1, 2$, $K = (k_1 + k_2)/2$ is the average momentum, $\Delta k_\mu = k_{1\mu} - k_{2\mu} = q_\mu$, x_i and k_i are the four coordinates for position and momentum variables respectively and ψ_i 's are the angles made by k_{iT} with the x-axis of each photon. The inclusion of the spin of the real photon will reduce the value of $C_2 - 1$ by 1/2.

We shall be presenting the results as functions of outward (q_{out}), side-ward (q_{side}) and longitudinal (q_{long}) momenta which can be expressed in terms of the transverse momentum of individual pair as follows [3];

$$q_{side} = \left| \vec{q}_T - q_{out} \frac{\vec{K}_T}{K_T} \right| = \frac{2k_{1T}k_{2T} \sqrt{1 - \cos^2(\psi_1 - \psi_2)}}{\sqrt{k_{1T}^2 + k_{2T}^2 + 2k_{1T}k_{2T} \cos(\psi_1 - \psi_2)}} \quad (4)$$

$$q_{out} = \frac{\vec{q}_T \cdot \vec{K}_T}{|K_T|} = \frac{(k_{1T}^2 - k_{2T}^2)}{\sqrt{k_{1T}^2 + k_{2T}^2 + 2k_{1T}k_{2T} \cos(\psi_1 - \psi_2)}} \quad (5)$$

$$q_{long} = k_{1z} - k_{2z} = k_{1T} \sinh y_1 - k_{2T} \sinh y_2 \quad (6)$$

where k_{iT} is the individual transverse momentum and y_i is the rapidity. It may be mentioned that the BEC function has values $1 \leq C_2(\vec{k}_1, \vec{k}_2) \leq 2$ for a chaotic source. These bounds are from quantum statistics. The source dimensions can be obtained by parameterizing the calculated correlation function with the empirical Gaussian form [2];

$$C_2(q, K) = 1 + \lambda \exp(-R_i^2 q_i^2) = 1 + \lambda \exp(-R_{side}^2 q_{side}^2 - R_{out}^2 q_{out}^2 - R_{long}^2 q_{long}^2) \quad (7)$$

where i stands for side, out and long. Thus R_{side} , R_{out} and R_{long} appearing in Eq. 7, are commonly referred to as HBT radii, which are measures of Gaussian widths of the source size. The deviation of λ from 1/2 will indicate the presence of non-thermal

sources, while the radius, R_{side} corresponding to q_{side} is closely related to the transverse size of the system. The radius, R_{out} corresponding to q_{out} measures both the transverse size and the duration of particle emission and R_{long} corresponding to q_{long} is the measure of longitudinal dimension of the system [3, 4, 21–23].

III. EMISSION RATE OF PHOTONS

A. Photon emission rate in anisotropic QGP

In the present work, the QCD annihilation ($q\bar{q} \rightarrow g\gamma$) and Compton ($q(\bar{q})g \rightarrow q(\bar{q})\gamma$) processes contribute to the photon spectra from QGP phase which has been calculated considering the quarks to be massive to avoid the divergence. The source function is related to the thermal emission rate of photons per unit four volume which is given by [18, 24]:

$$\begin{aligned} E \frac{dR}{d^3k} &= \frac{\mathcal{N}}{2(2\pi)^3} \int \frac{d^3p_1}{2E_1(2\pi)^3} \frac{d^3p_2}{2E_2(2\pi)^3} \frac{d^3p_3}{2E_3(2\pi)^3} \\ &\times (2\pi)^4 \delta^{(4)}(p_1 + p_2 - p_3 - k) |\overline{\mathcal{M}}|^2 \\ &\times f_1(\mathbf{p}_1, p_{hard}, \xi) f_2(\mathbf{p}_2, p_{hard}, \xi) \\ &\times [1 \pm f_3(\mathbf{p}_3, p_{hard}, \xi)] \end{aligned} \quad (8)$$

where \mathcal{N} is the over all degeneracy for the reactions under consideration, $|\overline{\mathcal{M}}|^2$ is the square of the invariant amplitude for the processes [25] under consideration (here $q\bar{q} \rightarrow g\gamma$ and $qg \rightarrow q\gamma$), f_i 's are the anisotropic distribution functions of the constituent partons in the medium.

In this work, we have assumed a system with a high momentum-space anisotropy where particles move in the specific direction. In such a scenario, the phase space distribution function can be obtained by compressing or stretching an arbitrary distribution along one direction in momentum space and can be expressed as follows [26]:

$$f(\mathbf{p}, \xi, p_{hard}) = f_{iso} \left(\sqrt{\mathbf{p}^2 + \xi(\mathbf{p} \cdot \mathbf{n})^2}, p_{hard} \right) \quad (9)$$

where \mathbf{n} is direction of anisotropy. As mentioned earlier, ξ is a parameter of momentum space anisotropy and p_{hard} is the hard momentum scale which is directly related to the average momentum of the partons. p_{hard} has a direct relevance with the temperature (T) of medium in isotropic scenario. We further assume that f_{iso} is the Fermi-Dirac (Bose-Einstein) distribution function for quarks (gluons). The anisotropy parameter ξ is related to transverse momentum (p_T) and longitudinal momentum (p_L) of the constituents via the following relation:

$$\xi = \frac{\langle p_T^2 \rangle}{2\langle p_L^2 \rangle} - 1 \quad (10)$$

When $\xi = 0$, the system is locally isotropic, but that does not imply the system to be in local thermal equilibrium unless f_{iso} is an equilibrium distribution function.

B. Photon emission rate from thermal medium

Beyond $\tau \geq \tau_{iso}$, thermal photons emerge just after the system thermalizes from both iQGP due to partonic interactions and from hot hadronic matter due to interactions among the hadrons. The rate of thermal photon production per unit space-time volume is given by [12, 15, 27] (see [13] for a review):

$$E \frac{dR}{d^3k} = \frac{g^{\mu\nu}}{(2\pi)^3} \text{Im}\Pi_{\mu\nu}^R f(E, T) \quad (11)$$

where $\text{Im}\Pi_{\mu\nu}^R$ is the imaginary part of the retarded photon self energy and $f(E, T)$ is the thermal phase space distribution. For an expanding system, the energy E should be replaced by $u_\mu k^\mu$, where k^μ and u^μ are the four momentum and the fluid four velocity respectively.

1. Photon emission rate in isotropic QGP

Thermal photons are produced from isotropic QGP with the interactions of the thermal quarks and gluons via QCD Compton and annihilation processes. To calculate the imaginary part of the photon self energy appearing in the Eq. 11 Hard Thermal Loops [28] approximation has been used. The complete calculation of the emission rate of photons from QGP to order $\mathcal{O}(\alpha_s)$ has been done by resumming the ladder diagrams in the effective theory [29].

2. Photon emission rate in hadronic phase

A set of hadronic reactions with all possible isospin combinations has been considered for the production of photons [30–32] from the hadronic matter. The effect of hadronic dipole form factors has been taken into account in the present work as in [32].

IV. SPACE-TIME EVOLUTION

For a dynamically evolving system the total photon yield can be evaluated by convoluting the static thermal emission rate (discussed in the previous section) with the expansion dynamics. In the present work the space time evolution is described as follows [24]. The system evolves anisotropically from

τ_i to τ_{iso} , where one needs to know the time dependence of $p_{hard}(\tau)$ and $\xi(\tau)$. We follow the work of ref [19] for the evolution in aQGP phase. As the radial flow is not developed properly in the initial stage of the collision, its effect is neglected in the anisotropic phase. For $\tau \geq \tau_{iso}$, the system is described by (1+2)d ideal hydrodynamics model with cylindrical symmetry [33] and boost invariance along the longitudinal direction [17]. Thus, the entire evolution is categorized as follows:

- When $\tau_i \leq \tau \leq \tau_{iso}$, the system evolves anisotropically and $p_{hard}(\tau)$ and $\xi(\tau)$ are the two time dependent parameters.
- When $\tau_{iso} \leq \tau \leq \tau_f$, the system becomes thermalized and evolves hydrodynamically with energy density (\mathcal{E}) and velocity as a function of space and time.

Hence, τ_{iso} is treated as free parameter in the calculation which controls the transition to the hydrodynamic scenario. However, it should be noted that by comparing with the data, it is possible to extract τ_{iso} as is done in case of single photon spectra [24] and nuclear modification factor for the light hadrons [34].

Thus, the one- and two- particle inclusive spectra can be presented as follows,

$$\begin{aligned} P_1(k) &= P_1^{aniso}(k) + P_1^{hydro}(k) \\ P_2(k_1, k_2) &= P_2^{aniso}(k_1, k_2) + P_2^{hydro}(k_1, k_2) \end{aligned} \quad (12)$$

P_i^{aniso} and P_i^{hydro} can be evaluated using Eqs. 2 and 3 with the help of space-time prescription for anisotropic and hydrodynamic scenario given in the following sections. Finally using Eq. 1 we obtain C_2 for the full evolution as well as for the individual phases.

In anisotropic prescription, P_i 's from an expanding system can be calculated by convoluting the static thermal emission rate ($\omega = EdR/d^3k$) with the expansion dynamics which depends on energy density, $\mathcal{E}(p_{hard}, \xi)$. Using Eq. 9 the parton energy density in an anisotropic plasma can be factorized in the following manner:

$$\mathcal{E}_0(p_{hard}, \xi) = \int \frac{d^3p}{(2\pi)^3} p^0 f(\mathbf{p}, \xi) = \mathcal{E}_{iso}(p_{hard}) \mathcal{R}(\xi) \quad (13)$$

where $\mathcal{R}(\xi) = [1/(\xi + 1) + \tan^{-1} \sqrt{\xi}/\sqrt{\xi}]/2$ and $\mathcal{E}_{iso}(p_{hard})$ is obtained by integrating the parton distribution functions (Eq. 9) for $\xi = 0$.

Now let us consider the space time evolution model for the aQGP to know the time dependence of ξ and p_{hard} . For this, we follow the works of Refs. [19, 20, 24]. According to this model there can be three possible scenarios : (i) $\tau_{iso} = \tau_i$, the

system evolves hydrodynamically so that $\xi = 0$ and p_{hard} can be identified with the temperature (T) of the system, (ii) $\tau_{iso} \rightarrow \infty$, the system never comes to equilibrium, (iii) $\tau_{iso} \geq \tau_i$ and τ_{iso} is finite, one should devise a time evolution model for ξ and p_{hard} which smoothly interpolates between pre-equilibrium anisotropy and hydrodynamics. This model can be executed mathematically by generalizing the anisotropic parameter $\xi(\tau)$ as follows;

$$\xi(\tau) = \left(\frac{\tau}{\tau_i} \right)^\delta - 1, \quad (14)$$

The limits $\delta = 0$ and $\xi = 0$ correspond to scenario (i) where expansion is hydrodynamical (thus iQGP corresponds to $\delta = 0$). On the otherhand, the limits $\delta \neq 0$ and $\xi \neq 0$ correspond to scenario (ii) where the system is highly anisotropic (thus aQGP corresponds to $\delta \neq 0$). For the present work we shall be following scenario (iii) which interpolates between hydrodynamic evolution and the anisotropic evolution. For constructing such an interpolating model, a transition width γ^{-1} is introduced to take into account the smooth transition from $\delta \neq 0$ to $\delta = 0$ at $\tau = \tau_{iso}$ (see Ref. [20] for details). The time dependence of various quantities are, therefore, obtained in terms of a smeared step function [19];

$$\lambda(\tau) = \frac{1}{2} (\tanh[\gamma(\tau - \tau_{iso})/\tau_i] + 1) \quad (15)$$

It is clear from the above equation that for $\tau \ll \tau_{iso}$, $\lambda \rightarrow 0$ (anisotropic evolution) and for $\tau \gg \tau_{iso}$, $\lambda \rightarrow 1$ (hydrodynamic evolution).

With this, the time dependence of relevant quantities are as follows [19, 20]:

$$\begin{aligned} \mathcal{E}(\tau) &= \mathcal{E}_0 [\mathcal{U}(\tau)/\mathcal{U}(\tau_i)]^{4/3}, \\ p_{hard}(\tau) &= T_i [\mathcal{U}(\tau)/\mathcal{U}(\tau_i)]^{1/3}, \\ \xi(\tau) &= a^{\delta[1-\lambda(\tau)]} - 1, \end{aligned} \quad (16)$$

where, $\mathcal{U}(\tau) \equiv [\mathcal{R}(a_{iso}^\delta - 1)]^{3\lambda(\tau)/4} (a_{iso}/a)^{1-\delta[1-\lambda(\tau)]/2}$, $a \equiv \tau/\tau_i$ and $a_{iso} \equiv \tau_{iso}/\tau_i$. The power of \mathcal{R} in \mathcal{U} keeps energy density continuous at $\tau = \tau_{iso}$ for all γ . In the present work, we have used a *free streaming interpolating* model that interpolates between early-time longitudinal free streaming and late-time ideal hydrodynamic expansion by choosing $\delta = 2$.

As mentioned earlier, in hydrodynamic prescription, P_i 's from an expanding system can be calculated by convoluting the static thermal emission rate ($\omega = EdR/d^3k$) with the expansion dynamics which depends on energy density ($\mathcal{E}(r, \tau)$) and radial ve-

locity ($v_r(r, \tau)$).

$$\begin{aligned}
P_1^{hydro}(k) &= \sum_i \int \omega_i(E^*, T) d^4x \\
P_2^{hydro}(k_1, k_2) &= P_1^{hydro}(k_1) P_1^{hydro}(k_2) + \\
&\sum_i \frac{1}{2} \int d^4x_1 d^4x_2 \omega_i(E^*, T) \omega_i(E^*, T) \cos(\Delta x^\mu \Delta k_\mu)
\end{aligned}
\tag{17}$$

The energy, E^* appearing in the thermal phase space factor, $f(E^*, T)$ (see Eq. 11) should be replaced by $k^\mu u_\mu$ for a system expanding with space-time dependent four velocity (u^μ). Assuming cylindrical symmetry and longitudinal boost invariance $k^\mu u_\mu$ can be expressed as

$$k^\mu u_\mu = \gamma_r(k_T \cosh(y - \eta) - v_r k_T \cos \phi), \tag{18}$$

where $v_r(\tau, r)$ is the radial velocity, $\gamma_r(\tau, r) = (1 - v_r(\tau, r)^2)^{-1/2}$.

The system produced in QGP phase reverts back to hot hadronic phase at a temperature $T \sim T_c$. Thermal equilibrium may be maintained in the hadronic phase until the mean free path remains comparable to the system size. In Eq.(17), i stands for qgp (Q), mixed phase (M) (in a 1st order phase transition scenario) and hadronic phase (H). Thus P_i 's for full hydrodynamic evolution can be obtained by summing the contribution from individual phase, where the contribution from each phase can be obtained by choosing the phase space appropriately.

The initial conditions are essential for ideal hydrodynamics and can be obtained by the following prescription [24].

$$\begin{aligned}
T_i^{hydro} &= p_{hard}(\tau_{iso}) \\
\tau_i^{hydro} &= \tau_{iso}
\end{aligned}
\tag{19}$$

The initial conditions are given through the energy density and velocity profile,

$$\begin{aligned}
\mathcal{E}(\tau_i, r) &= \frac{\mathcal{E}_0(\xi = 0, T_i^{hydro})}{1 + \exp(\frac{r-R_A}{\sigma})} \\
v_r(\tau_i, r) &= v_0 \left(1 - \frac{\mathcal{E}_0(\xi = 0, T_i^{hydro})}{1 + \exp(\frac{r-R_A}{\sigma})} \right)
\end{aligned}
\tag{20}$$

where $\mathcal{E}_0(\xi = 0, T_i^{hydro})$ is the initial energy density which is related to initial temperature (T_i^{hydro}). Here R_A is the nuclear radius and σ is the diffusion parameter and taken as 0.5 fm. We have taken the transition temperature $T_c = 175$ MeV and fixed the freeze-out temperature $T_f = 120$ MeV. For the QGP and the hadronic phases lattice QCD EoS [35] (for $T > T_c$) and hadronic resonance gas EoS [36] (for

$T < T_c$) have been used respectively. For the transition region we have used the following parameterization [37];

$$\begin{aligned}
s(T) &= s_q(T) f_q(T) + [1 - f_q(T)] s_h(T), \\
f_q(T) &= \frac{1}{2} (1 + \tanh \frac{T - T_c}{\Gamma})
\end{aligned}
\tag{21}$$

where Γ is the width parameter and assumes a finite value for the crossover transition and for the first order transition this value can be tuned to zero. Here the width parameter is taken to be $\Gamma = 25$ MeV.

V. RESULTS

With all these ingredients discussed in the previous sections we have evaluated the two-photon correlations as a function of q_{out} , q_{side} and q_{long} for two sets of RHIC initial conditions. In both the cases for $\tau_{iso} > \tau_i$, we have observed a reduction of C_2 for anisotropic scenario compared to that of in isotropic case by incorporating the initial momentum anisotropy. We choose τ_{iso} in such a way that one of the values corresponds to the isotropic situation ($\tau_{iso} = \tau_i$) and others corresponds to anisotropic scenario ($\tau_{iso} > \tau_i$). So basically we have attempted to examine the sensitivity of momentum anisotropy on C_2 by controlling the variable, τ_{iso} . The corresponding HBT radii can be extracted with the help of the parametrization expressed in Eq. 7 and can be compared with the data to extract τ_{iso} .

A. C_2 as function of q_{out}

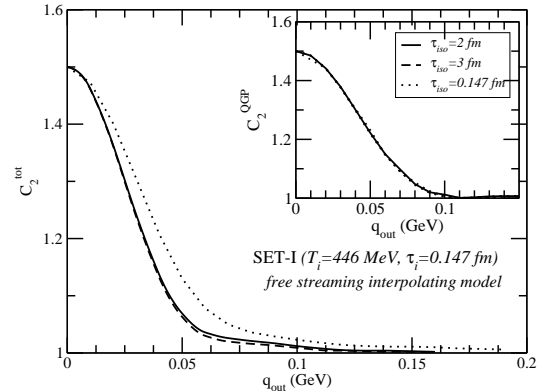


FIG. 1: Correlation function for photon pairs as a function of q_{out} for SET-I ($T_i = 446$ MeV and $\tau_i = 0.147$ fm/c) is plotted with different τ_{iso} and the inset figure is same for QGP (aQGP+iQGP) phase only.

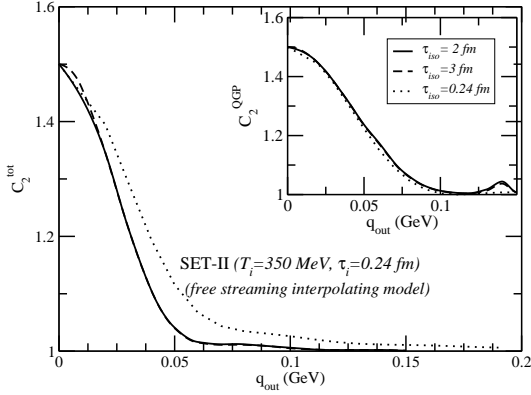


FIG. 2: Correlation function for photon pairs as a function of q_{out} for SET-II ($T_i = 350$ MeV and $\tau_i = 0.24$ fm/c) is plotted with different τ_{iso} and the inset figure is same for QGP (aQGP+iQGP) phase only.

By taking $\psi_1 = \psi_2 = 0$, $y_1 = y_2 = 0$ and fixing the transverse momentum of one photon ($k_{1T} = 2$ GeV) and varying the other (k_{2T}), we obtain C_2 as a function of q_{out} . In Figs. 1 and 2, we have plotted the variation of C_2 as a function of q_{out} in full evolution scenario with SET-I and SET-II initial conditions respectively. From both the figures, we infer that varying τ_{iso} , a considerable shift is observed in C_2 . With increasing τ_{iso} , the value of R_{out} (see table I) which corresponds to q_{out} increases. This happens because by increasing τ_{iso} , the system expands slower to achieve thermalization and isotropization. Whereas in the inset of Figs.1 and 2 which describe C_2 for the QGP (aQGP+isotropic QGP) phase, substantial change is not observed unlike the case for C_2^{tot} . This happens because the flow is not developed in early QGP phase and with the progress of time the thermal energy is transformed into flow energy in later stage of the collision, so flow is fully developed in the hadronic stage [11, 16] resulting in reduction of R_{out} by increasing τ_{iso} . The reduction is mostly affected due to the radial flow as well as the τ_{iso} dependent initial conditions for hydrodynamic evolution which is due to the inclusion of momentum space anisotropy.

B. C_2 as function of q_{side}

By taking $k_{1T} = k_{2T} = 2$ GeV, $y_1 = y_2 = 0$ and fixing $\psi_2 = 0$ and varying ψ_1 , we obtain C_2 as a function of q_{side} . In Figs. 3 and 4, we have plotted the variation of C_2 as a function of q_{side} for the full evolution scenario with SET-I and SET-II initial conditions respectively. From both the figures, it is observed that C_2 is shifted towards left considerably. By increasing τ_{iso} , the value of R_{side}

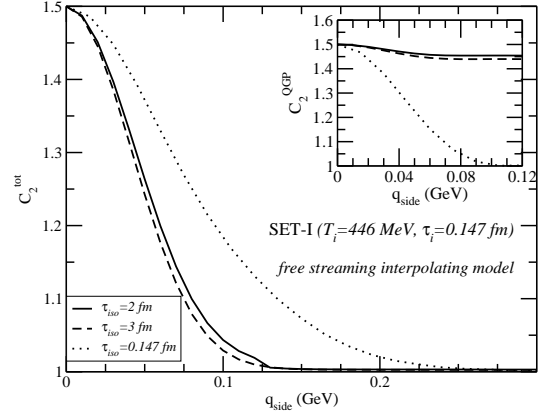


FIG. 3: Correlation function for photon pairs as a function of q_{side} for SET-I ($T_i = 446$ MeV and $\tau_i = 0.147$ fm/c) is plotted with different τ_{iso} and the inset figure is same for QGP (aQGP+iQGP) phase only.

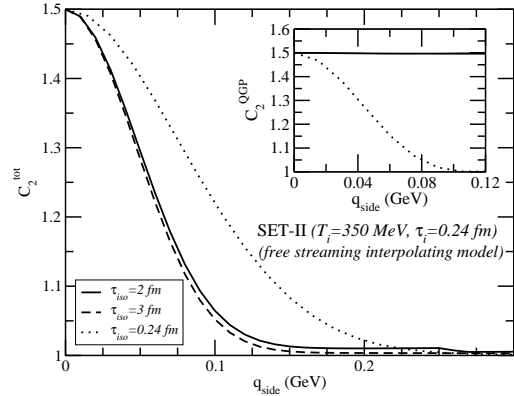


FIG. 4: Correlation function for photon pairs as a function of q_{side} for SET-II ($T_i = 350$ MeV and $\tau_i = 0.24$ fm/c) is plotted with different τ_{iso} and the inset figure is same for QGP (aQGP+iQGP) phase only.

(see table I) which corresponds to q_{side} is also enhanced. This happens because by increasing τ_{iso} , the system expands slower to achieve thermalization and isotropization. Whereas C_2 for the QGP (aQGP+isotropic QGP) phase depicted in the insets of Figs.3 and 4 shows an opposite behaviour compared to that observed in the full evolution scenario. In other words, by increasing τ_{iso} the values of R_{side} increase in full evolution scenario whereas it decrease in the QGP phase. It can be shown that $R_{side} \sim 1/(1 + E_{collective}/E_{thermal})$ [2], where $E_{thermal}$ depends inversely on τ_{iso} . In addition to it, the flow is not developed properly in the QGP phase, so $E_{collective} \ll E_{thermal}$. Thus, with the increase of τ_{iso} the ratio $E_{collective}/E_{thermal}$ increases. As a result the value of R_{side} decreases. Whereas in

the hadronic phase, the flow is fully developed resulting in $E_{collective} \gg E_{thermal}$. The thermal energy is reduced even more by increasing τ_{iso} . So due to the radial flow effect the values of R_{side} increase with the increase in the values of τ_{iso} in the full evolution scenario.

C. C_2 as function of q_{long}

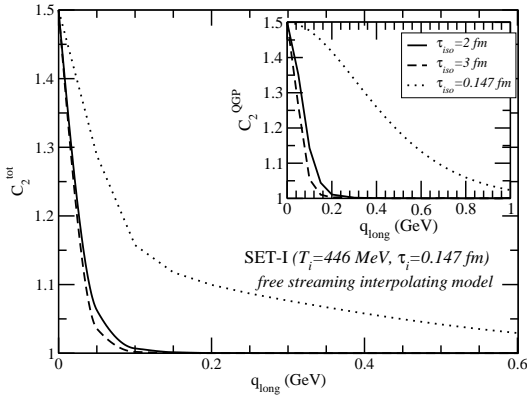


FIG. 5: Correlation function for photon pairs as a function of q_{long} for $T_i = 446$ MeV and $\tau_i = 0.147$ fm/c and the inset figure is same for QGP (aQGP+iQGP) phase only.

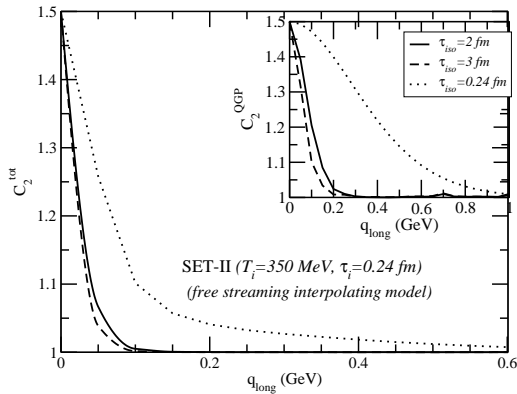


FIG. 6: Correlation function for photon pairs as a function of q_{long} for $T_i = 350$ MeV and $\tau_i = 0.24$ fm/c and the inset figure is same for QGP (aQGP+iQGP) phase only.

C_2 as a function of q_{long} can be obtained by taking $\psi_1 = \psi_2 = 0$, $k_{1T} = k_{2T} = 2$ GeV and taking one of the photons at mid-rapidity ($y_1 = 0$) and varying the other (y_2). The variation of C_2 as a function of q_{long} with SET-I and SET-II initial conditions for RHIC energy is shown in Figs. 5 and 6 respectively.

It is clear from both the figures that there is a considerable difference for isotropic (when $\tau_{iso} = \tau_i$) and anisotropic (for $\tau_{iso} = 2, 3$ fm/c) scenarios. It is argued previously that the anisotropy in momentum space arises due to $\langle p_L^2 \rangle \ll \langle p_T^2 \rangle$. Thus we can argue here that the difference arises in size in the longitudinal direction because of the above said asymmetry in momentum space. Hence R_{long} increases (see Table I) with the increase of τ_{iso} .

D. Source Dimensions

TABLE I: The values of R_{out} , R_{side} and R_{long} obtained from C_2 (using Eq. 7) is tabulated below.

T_i (MeV)	τ_{iso} (fm/c)	R_{out} (fm)	R_{side} (fm)	R_{long} (fm)
446	0.147	4.5	1.95	2.6
	2.0	5.5	3.13	6.6
	3.0	5.6	3.34	6.8
350	0.24	4.69	1.77	2.9
	2	6.08	2.83	6.3
	3	6.09	2.96	6.7

We would like to mention here that the HBT radii give the length of homogeneity of the source and this is equal to the geometric size if the source is static. The HBT radii obtained from C_2 using Eq. 7 is tabulated in Table. I. However, for a dynamic source, e.g., for the system formed after ultra-relativistic heavy ion collisions, the HBT radii are smaller than the geometric size. Figuring out the numbers tabulated in Table. I, it is clear that the HBT radii increase with the inclusion of anisotropy, i.e., with increasing τ_{iso} . Also a remarkable change in HBT radii is observed in the QGP phase (for both R_{side} and R_{long}) with the inclusion of momentum space anisotropy except the outward direction.

VI. SUMMARY

In this work, we have attempted to evaluate the correlation function, C_2 for two identical photons as functions of q_{out} , q_{side} and q_{long} for RHIC energy with two sets of initial conditions and with initial state momentum space anisotropy. Hence R_{out} , R_{side} and R_{long} extracted from C_2 in such a scenario provide us the spatial informations of the evolving system. In summary, we have shown that C_2 for QGP phase doesn't change appreciably with q_{out} for both sets of initial conditions used here. For the entire evolution, we do observe an appreciable change

in the variation of C_2 as a function of q_{out} due to the effect of radial flow and τ_{iso} dependent initial conditions for hydrodynamic evolution. We also observe a significant change for both the QGP phase and full evolution for the initial momentum space anisotropy when C_2 is plotted as a function of q_{side} . The most interesting results are obtained in the variation of C_2 along the longitudinal direction because of the asymmetry in $p_T - p_L$ plane. As $\langle p_L^2 \rangle \ll \langle p_T^2 \rangle$, the maximal effect of momentum anisotropy is observed and correspondingly R_{long} changes quite substantially with τ_{iso} for both sets of initial conditions. Hence, it is observed that by increasing the values of τ_{iso} , all the HBT radii increases in full evolution scenario considerably due to effect of initial momentum anisotropy and the radial flow as well. However, in the QGP phase it affects only in side-ward and longitudinal directions. These are the most remarkable

results that have been obtained in this work by introducing initial state momentum anisotropy. Finally, it is to be noted that we have not considered the fact that how much fractions of iQGP and aQGP are there during the transition from aQGP to iQGP at $\tau = \tau_{iso}$. Although, in principle, this aspect should be considered during this transition. This concept will be incorporated in the lepton-pair interferometry and work in this line is in progress [38]. It is also straight forward to extend this analysis to LHC energies.

VII. ACKNOWLEDGMENT:

P M and M M want to thank L. Bhattacharya for useful discussion.

-
- [1] R. Hanbury Brown and R. Q. Twiss, Nature **178**, 1046(1956) .
- [2] S. Pratt, Phys. Rev. **D 33**, 1314 (1986).
- [3] U. A. Weidemann and U. Heinz, Phys. Rep. **319**, 145 (1999).
- [4] U. Heinz and B. V. Jacak, Ann. Rev. Nucl. Part. Sci. **49**, 529 (1999); T. Csörge and B. Lörstad, Phys. Rev. C **54**, 1390 (1996); B. R. Schlei and N. Xu, Phys. Rev. C **54**, R2155 (1996); D. H. Rischke and M. Gyulassy, Nucl. Phys. A **608**, 479 (1996).
- [5] D. Peressounko, Phys. Rev. C **67**, 014905 (2003).
- [6] E. Frodermann, U. Heinz, Phys. Rev. C **80** 044903 (2009).
- [7] J. Alam, B. Mohanty, P. Roy, S. Sarkar and B. Sinha Phys. Rev. C **67**, 054902 (2003).
- [8] S. A. Bass, B. Mueller and D. K. Srivastava, Phys. Rev. Lett. **93**, 162301 (2004).
- [9] D. K. Srivastava and J. I. Kapusta, Phys. Lett. B **319**, 407 (1993); D. K. Srivastava, Phys. Rev. D **49**, 4523 (1994).
- [10] D. K. Srivastava and R. Chatterjee, Phys. Rev. C **80**, 054914 (2009).
- [11] P. Mohanty, J. Alam and B. Mohanty, Phys. Rev. C **84**, 024903 (2011); P. Mohanty, J. Alam and B. Mohanty, Nucl. Phys. A **862** 301-303, (2011). P. Mohanty, J. Alam, PoS(WPCF2011)**040**, (2012), arXiv : 1202.2189[Nucl-th].
- [12] L. D. McLerran and T. Toimela, Phys. Rev. D **31**, 545 (1985).
- [13] J. Alam, S. Raha and B. Sinha, Phys. Rep. **273**, 243 (1996).
- [14] J. Alam, S. Sarkar, P. Roy, T. Hatsuda and B. Sinha, Ann. Phys. **286**, 159 (2001).
- [15] C. Gale and J.I. Kapusta, Nucl. Phys. B **357**, 65 (1991).
- [16] P. Mohanty, J. K. Nayak, J. Alam and S. K. Das, Phys. Rev. C **82** 034901 (2010).
- [17] J. D. Bjorken, Phys. Rev. D **27**, 140 (1983).
- [18] B. Schenke and M. Strickland Phys. Rev. D **76**, 025023 (2007).
- [19] M. Martinez and M. Strickland, Phys. Rev. Lett. **100**, 102301 (2008).
- [20] M. Martinez and M. Strickland, Phys. Rev. C **78**, 034917 (2008).
- [21] D. H. Rischke and M. Gyulassy, Nucl. Phys. A **608**, 479 (1996).
- [22] M. Herrmann and G. F. Bertsch, Phys. Rev. C **51**, 328 (1995).
- [23] S. Chappman, P. Scotto and U. Heinz, Phys. Rev. Lett. **74**, 4400 (1995).
- [24] L. Bhattacharya and P. Roy, Phys. Rev. C **78**, 064904 (2008), L. Bhattacharya and P. Roy, Phys. Rev. C **79**, 054910 (2009).
- [25] C. Y. Wong and H. Wang, Phys. Rev. C **58**, 376 (1998).
- [26] P. Romatschke and M. Strickland, Phys. Rev. D **69**, 065005 (2004).
- [27] H.A. Weldon, Phys. Rev. D **42**, 2384 (1990).
- [28] E. Braaten and R. D. Pisarski, Nucl. Phys. B **337**, 569 (1990) ; *ibid* **339**, 310 (1990) .
- [29] P. Arnold, G.D. Moore, and L.G. Yaffe, J. High Energy Phys. **0111**, 057 (2001); P. Arnold, G.D. Moore, and L.G. Yaffe, J. High Energy Phys. **0112**, 009 (2001); P. Arnold, G.D. Moore, and L.G. Yaffe, J. High Energy Phys. **0206**, 030 (2002).
- [30] S. Sarkar, J. Alam, P. Roy , A. K. Dutt-Mazumder, B. Dutta-Roy, B. Sinha, Nucl. Phys. A **634**, 206 (1998).
- [31] P. Roy, S. Sarkar, J. Alam and B. Sinha, Nucl. Phys. A **653**, 277 (1999).
- [32] S. Turbide, R. Rapp and C. Gale, Phys. ReV. C **69**, 014903 (2004) .
- [33] H. von Gersdorff, M. Kataja, L. McLerran and P. V. Ruuskanen, Phys. Rev. D **34**, 794 (1986).
- [34] M. Mandal, L. Bhattacharya and P. Roy, Phys. Rev. C **84**, 044910 (2011).
- [35] C. Bernard *et al.*, Phys. Rev. D **75** 094505 (2007).
- [36] B. Mohanty and J. Alam, Phys. Rev. C **68**, 064903

- (2003).
- [37] M. Asakawa and T. Hatsuda, Phys. Rev. D **55**, 4488 (1997).
- [38] P. Mohanty *et.al.* [work in progress].